CHAPTER 4

STUDY ON THE ELETRON BEAM OF THE TRANSIENT HOLLOW CATHODE DEVICE.

A two-dimensional spatial potential distribution is calculated by solving the Laplace's equation in cylindrical coordinate system and tracing the electric field lines inside a hollow cathode device geometry. The transient hollow cathode discharge (THCD) is known to have pd values at the left hand branch of the Paschen curve. This means at different pressure the intensity of electron beam will be affected. According to Gastel *[M. Gastel, et al., 1995]*, the volume of the hollow cathode is also a factor that will affect the production of charge carriers. It is also observed that the use of different kind of working gas will also affect the intensity of the electron beam. But at lower pressure, the inter-electrode gas is not expected to play an important role *[P. Choi, et al, 1987]*. In the present study, the effect of pressure variation on the system and the diameter of the hollow cathode on the electron beam have been studied. By using the 24 μm aluminised mylar foil in combination with 10 μm copper foil, and using carbon disc as the bombardment target, the electron beam energy has been measured.

4.1 Mapping The Potential And Electric Field Lines In The Transient Hollow Cathode Device

An attempt is made to compute the electric field distribution for the THCD geometry. In order to obtain the electric field lines distribution in vacuum, the Laplace's equation in cylindrical co-ordinates is used as follow :

$$\nabla^2\phi(r,z,\theta) = 0 \tag{4.1}$$

where $\phi(r, z, \theta)$ is the potential at a point (r, z, θ) in space. For the hollow cathode geometry with cylindrical symmetry (i.e., independent of θ), equation 4.1 can be written as

$$\frac{\partial^2\phi}{\partial r^2} + \frac{\partial^2\phi}{\partial z^2} + \frac{1}{r}\frac{\partial\phi}{\partial r} = 0 \tag{4.2}$$

This equation can be solved numerically using the relaxation method in two dimensions. The r-z plane in space is divided into $n \times m$ grid points, each separated by a distance Δ. The anode and cathode are assumed to have constant potentials ϕ and ϕ_c respectively. These potentials constitute the boundary. Figure 4.1 shows the position of the grid points for the present system, where i indicates the row and j is the column index.

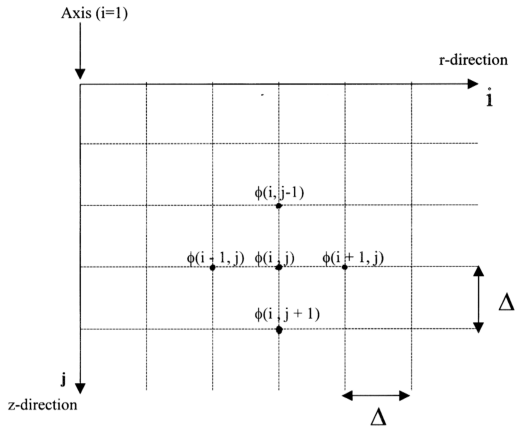

Figure 4.1 The definition of grid point potentials.

Referring to Figure 4.1 with square mesh of spacing Δ, the various terms of the Laplace equation are then given as:

$$\frac{\partial^2 \phi}{\partial r^2} = \frac{\phi_{i+1,j} - 2\phi_{i,j} + \phi_{i-1,j}}{\Delta^2}$$

$$\frac{\partial^2 \phi}{\partial z^2} = \frac{\phi_{i,j+1} - 2\phi_{i,j} + \phi_{i,j-1}}{\Delta^2}$$

and

$$\frac{1}{r}\frac{\partial \phi}{\partial r} = \frac{\phi_{i+1,j} - \phi_{i-1,j}}{2(i-1)}$$

where i=1 at the axis. Taking the finite difference approximation for the Laplace's equation with $i \approx 1$, where it is corresponding to the axis (r=0) with a square mesh of spacing Δ, the potential ϕ at any normal interior grid point (i, j) is obtained from

$$4\phi_{i,j} = \left\{1 + \frac{1}{2(i-1)}\right\}\phi_{i+1,j} + \left\{1 - \frac{1}{2(i-1)}\right\}\phi_{i-1,j} + \phi_{i,j+1} + \phi_{i,j-1} \tag{4.3}$$

while the potential at the axis $\phi(1,j)$ is given by

$$6\phi(1,j) = \phi(1,j+1) + \phi(1,j-1) + 4\phi(2,j). \tag{4.4}$$

Each grid point is re-calculated for every iteration. The iteration is repeated until the potential at the individual grid point converges, that is $\phi_N(i,j) \approx \phi_{N-1}(i,j)$. N is the total number of iteration for the calculation to converge. The cut-off point has been chosen when $0.999 < \phi_N(i,j)/\phi_{N-1}(i,j) < 1.001$.

The position, (i',j'), of equal potential Φ, are joined to form an equipotential contour. If (i',j') lies between (i,j) and (i+1,j), its position will be linearly interpolated by using the following relation

$$i' = i + \frac{|\Phi - \phi_N(i,j)|}{|\phi_N(i+1,j) - \phi_N(i,j)|}$$

$$j' = j$$

or for (i',j') lies between (i,j) and (i,j+1),

$$j' = j + \frac{|\Phi - \phi_N(i,j)|}{|\phi_N(i,j+1) - \phi_N(i,j)|}$$

$$i' = i$$

The above relaxation method can be implemented by using the Microsoft Excel spreadsheet whereby each cell is used to represent a grid point in two dimensional space. Each cell contains either a formula (equation 4.4) or a constant value such as the boundary value. In the present study, the cathode boundary is initially assigned with a specific potential V_{INIT}, that is -60 kV, whilst the anode boundary is at 0 voltage. As the electric field distribution is symmetrical about the z-axis (in a cylindrical co-ordinate system), it is sufficient to represent only half of the cross-sectional plane of interest. The size of the spreadsheet used is 108 cells (r-direction) by 242 cells (z-direction) being scaled from (24×56)mm. The distance between adjacent r-cells and z-cells is $\Delta = 0.2222$.

Figure 4.2 shows the electric potential contour for the present system with inter-electrode spacing of 21 mm, hollow cathode size of 5 mm and cathode voltage of -60 kV. It is clearly shown that the equipotential line of -50 kV is formed along the border of the hollow cathode. After the equipotential line of -500 V, there is no influence of the hollow cathode to the equipotential line.

From the grid point potential, the average electric fields in the radial direction E_r and axial direction E_z are calculated at every grid point (i,j) according to the following equations,

$$E_r(i,j) = \frac{\phi_N(i,j+1) - \phi_N(i,j-1)}{2\Delta}, \tag{4.5}$$

$$E_z(i,j) = \frac{\phi_N(i+1,j) - \phi_N(i-1,j)}{2\Delta} \tag{4.6}$$

resulting in the magnitude of the electric field E at grid point (i,j) as

$$E(i,j) = \sqrt{E_r^2(i,j) + E_z^2(i,j)} \tag{4.7}$$

E(i, j) is high along the axis. The magnitude of the electric field along the axis is the cause of the electron beam formation. The tracing of the electron path is carried out by using the Automated Streamline Analysis. This method was originally used to trace the wind direction on the earth surface *[T. M. Whittaker, 1976]*.

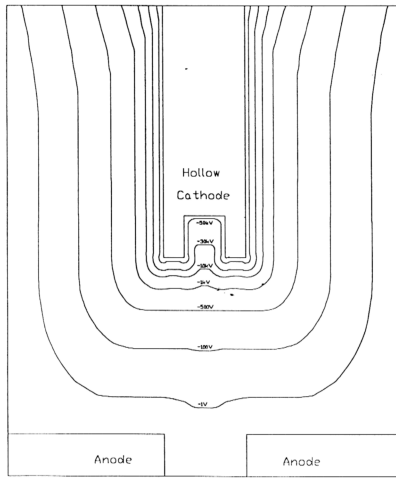

Figure 4.2 The potential contour computed for THCD system.

The electric field line can be drawn starting from a chosen grid-point (r, z), which is taken to be located immediately next to the surface of the cathode to represent the emergence point of an electron, by finding the next position where the line will be ended, $(r+D_r, z+D_z)$, where

$$D_r = \frac{E_r}{E} D,$$

$$D_z = \frac{E_z}{E} D$$

This procedure is repeated from the new position of the electric field line until it ends at the anode or at the edge of the representative cell area (in the case of runaway electron).

When the line passes through a point (r, z) which is located in the rectangular space surrounded by four grid points, as shown in Figure 4.3, the value of E is chosen from either one of the grid points by inspection to determine which grid point is the shortest distance by referring to the following criteria:

1.) if $\Delta r \leq 0.5\Delta$ and $\Delta z \leq 0.5\Delta$, E(i, j) is chosen ;

2.) if $\Delta r \geq 0.5\Delta$ and $\Delta z \leq 0.5\Delta$, E(i, j+1) is chosen ;

3.) if $\Delta r \leq 0.5\Delta$ and $\Delta z \geq 0.5\Delta$, E(i+1, j) is chosen ; and

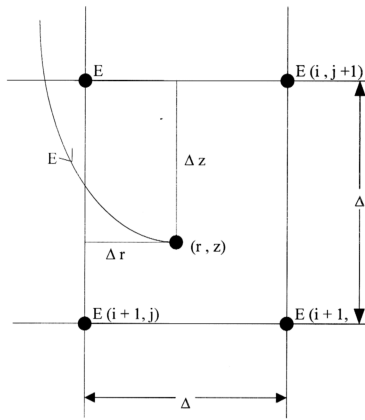

Fig. 4.3 The trace of electric field line when entering into a position in between the grid points.

4.) if $\Delta r \geq 0.5\Delta$ and $\Delta z \geq 0.5\Delta$, E(i+1, j+1) is chosen.

The electric field lines for the present system with inter-electrode spacing of 21 mm, hollow cathode size of 5 mm and cathode voltage of -60 kV are shown in Figure 4.4. It can be observed that the field is highest along the axis of the system. The electric field lines are found to extend into the hollow cathode region. The intensity of the electric field is higher around the edge of the opened end of the hollow cathode. The distribution of the electric field lines is more intense inside the center hollow cathode region. Any electron that is generated in the hollow cathode region will be focussed and accelerated by the electric field towards the anode.

For the discharge without triggering means, the initial electrons will be released from the cathode surface in the hollow cathode region by a random process caused by stray radiation, probably the cosmic ray, or the initial electrons are forced to release by a electric field which increases to -60 kV in several ns. These electrons will then ionize the gas by collisional ionization *[Townsend, 1901]*. After numerous collisions, avalanche will occur. The electrons which are produced from the avalanche are focused by the electric field to form an electron beam leading to electrical breakdown. The presence of the electron beam is evident from Figure 4.5 where the electron beam bombard the carbon target and produce X-ray.

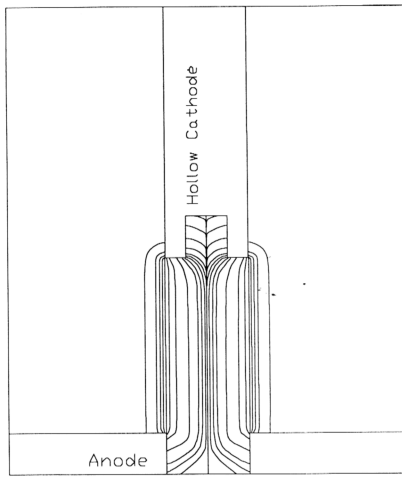

Figure 4.4 The electric field lines mapping for the THCD system.

4.2 The Effect Of Pressure And Charging Voltage

The effect of pressure on the production and enhancement of electron beam of the THCD has been investigated. The THCD is operated at voltages of –40 kV, -50 kV and -60 kV powered by a 2-stage Marx circuit. The operating pressure has been varied from 4.0 x 10^{-3} to 4.0 x 10^{-2} mbar. The diameter and the length of the hollow cathode are 5 mm and 12.5 mm respectively. Copper and carbon are used as the electron beam bombardment target and BPX-65 PIN diodes, which are covered by 12 μm aluminised mylar, are used to detect the X-rays produced.

Figure 4.5 shows the PIN diode output signals obtained together with the rate of change of the discharge current, dI/dt, for discharges at -60 kV with different pressures. As can be observed, the intensity of X-ray pulse is low and broad at low pressure, indicating low intensity electron beam emission lasting for about 500 ns. When the pressure is increased, the intensity of X-ray signal also increases. At the optimum pressure of 1.5 x 10^{-2} mbar, X-ray pulse of maximum intensity is obtained. The X-ray pulse is observed to rise sharply within a few nanoseconds. The duration of the X-ray pulse lasts for about 120 ns. Further increase in pressure will cause the intensity of X-rays to decrease. No X-rays are detected at pressure of 4.0 x 10^{-2} mbar. The rise of the dI/dt signal is found to be affected by the pressure. The slow rise time of the dI/dt at low pressure indicates that the plasma is resistive at the start of the discharge. The rise time is sharper at the pressure of 4.0x10^{-2} mbar. This shows that the plasma is heated up more rapidly at this pressure.

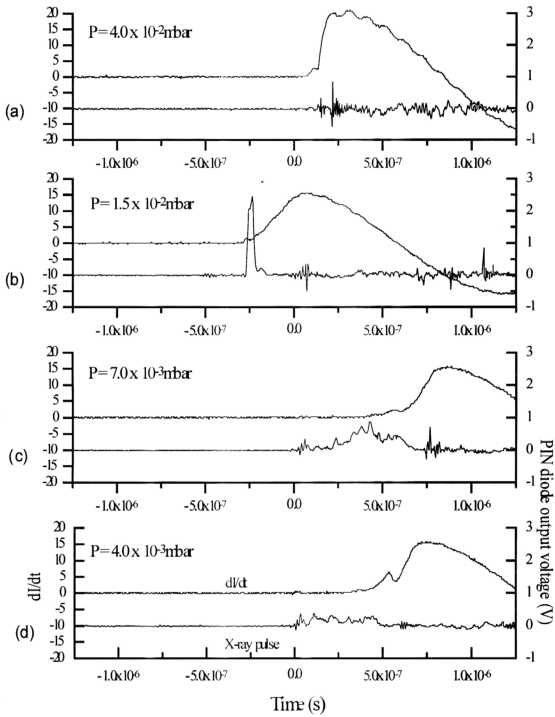

Figure 4.5 X-ray pulses and dI/dt signals obtained for discharges at –60 kV with different pressures.

Figure 4.6 shows the PIN diode signals together with the dI/dt signals obtained at a discharge voltage -50 kV at different pressures. It is observed that the X-ray intensity in Figure 4.6 is lower than that in Figure 4.5, which are discharges at -60 kV. This indicates that higher charging voltage applied to the system will produce higher energy electron beam during the pre-breakdown phase. This is consistent with the fact that the electron beam is produced before breakdown occurs. When the discharge voltage further decreases to -40 kV, the intensity of the X-ray generated is too low to be detected by the PIN diode.

In another series of experiments, copper is used as the electron beam bombardment target. The results are shown in Figure 4.7. The discharge voltage is –50 kV, which is similar to the discharge condition used in Figure 4.6. The maximum of the X-ray intensity is about 13 V at pressure of 1.5×10^{-2} mbar. The X-ray pulses have much shorter duration compared to those for carbon target as shown in Figure 4.6. The X-ray pulse can still be observed at pressure of 4.0×10^{-2} mbar. In Figure 4.6 (c) and (d), the X-ray signals are broad and this may be due to the several 'burst' of low energy electron beams from the hollow cathode.

The above results can be compared to earlier results obtained from UMFX-II *[C.S. Wong, et. al, 1992]*. This system was operated at discharge voltage of 40 kV powered by a 2-stage MARX capacitor circuit of 1.65 nF. The operating pressure has been varied from 10^{-1} mbar to 10^{-4} mbar. The bombardment target, which is the anode, is made of stainless steel. The cathode is a stainless steel disc with a hole at the center which is tapered towards the anode. A set of results from UMFX-II is

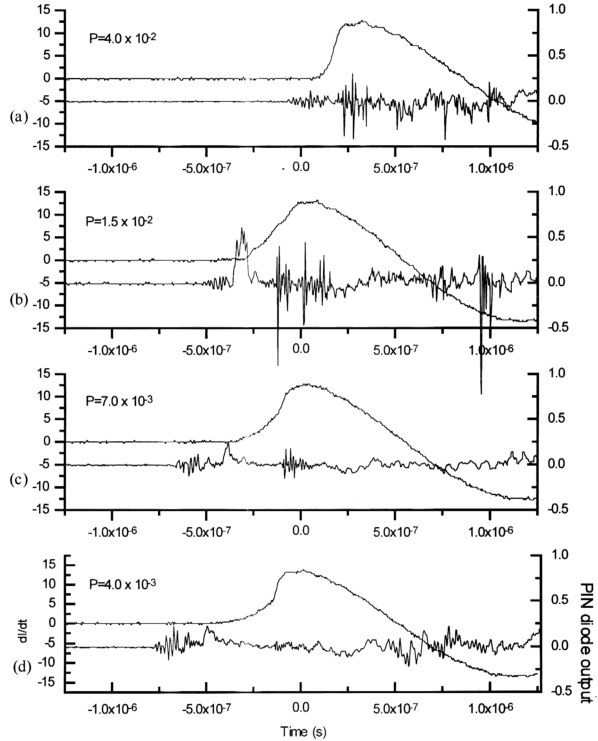

Figure 4.6 X-ray pulses and dI/dt signals obtained for discharges at –50 kV with different pressures.

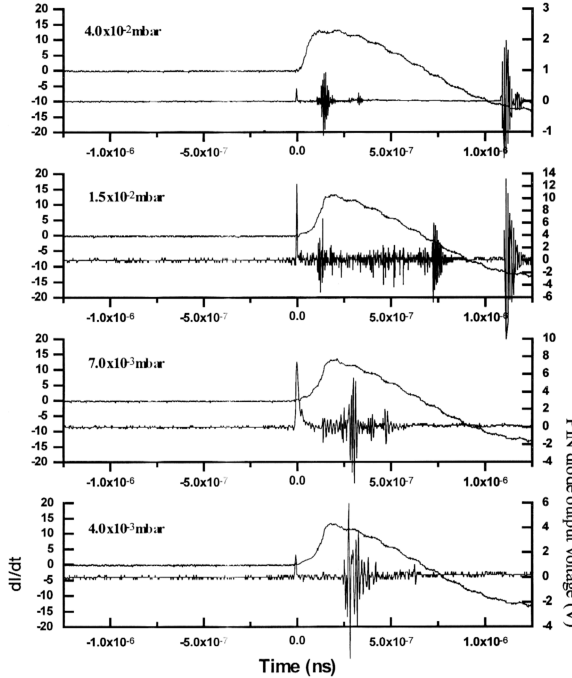

Figure 4.7 X-ray pulses and dI/dt signals obtained from the copper target for discharges at –50 kV with different pressures .

reproduced in Figure 4.8. The following observations can be obtained from the comparison : (a) At low pressure, the dI/dt signals are observed to be rising more slowly in both cases. (b) The intensity of the X-ray pulse and the duration of the beam production from UMFX-II increase as the pressure decrease and no optimum X-ray intensity can be observed within the pressure range of 10^{-1} to 10^{-4} mbar, whereas in this project, the electron beam production is optimum at a pressure of 1.5×10^{-2} mbar.

4.3 Influence Of The Hollow Cathode Diameter On The Electron Beam

The influence of the diameter of the hollow cathode on the generation of electron beam has been investigated by using 2 hollow cathodes, one with a diameter 1.5 mm and another one with a diameter 5 mm. Both hollow cathodes have a depth of 12.5 mm. Brass is used as the target for the detection of the electron beam. The detector used is the PIN diode model 100-PIN-250.

In order to investigate the effect of the diameter of the hollow cathode on the electron beam generation, two series of experiments, one with d = 1.5 mm and another with d = 5 mm were carried out. Figure 4.9 shows the PIN diode output pulses obtain at different pressures ranging from 2.0×10^{-3} mbar to 3.0×10^{-2} mbar for d = 1.5 mm. The discharge voltage is at -50 kV. At pressure of 2.0×10^{-3} mbar, the intensity of the X-ray emission is about 0.9 V. When the pressure is lower than

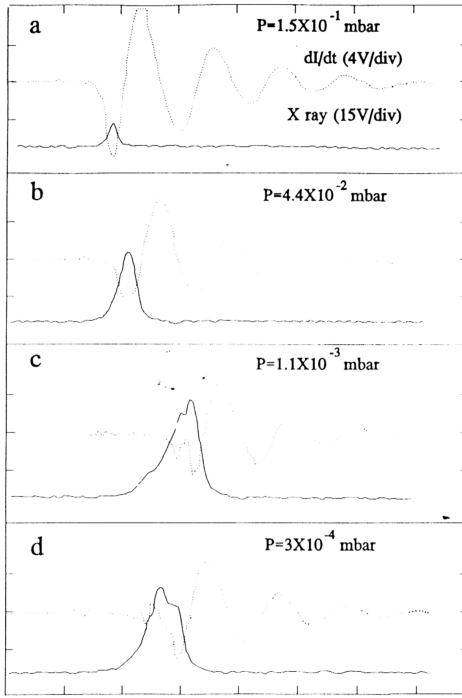

Figure 4.8 Reproduce results of UMFX-II for 40kV discharge at various pressures *[C. S. Wong, et.al., 1992]*

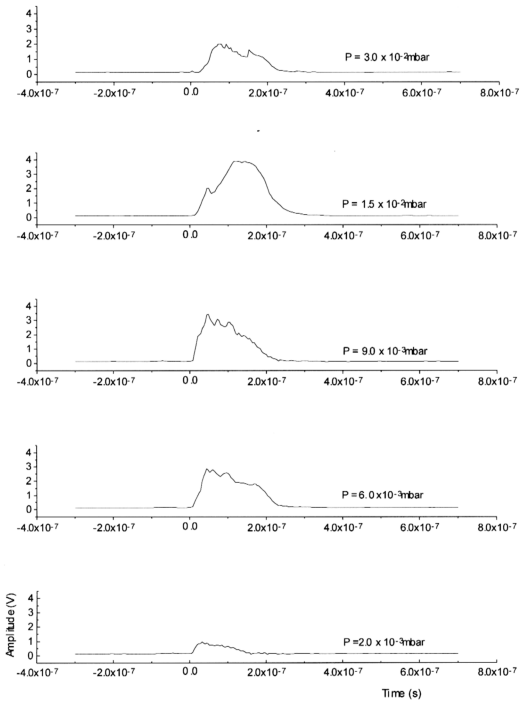

Figure 4.9 PIN diode output voltage obtained at various pressures for 1.5 mm diameter hollow cathode.

2.0×10^{-3} mbar, no X-ray is detected. The intensity of the electron beam increases when the pressure increases until it reaches the optimum pressure, 1.5×10^{-2} mbar, where the amplitude is 3.9 V. Further increase in the pressure will cause the intensity of the X-ray pulse to decrease.

Figure 4.10 shows another series of discharges using similar parameters as in Figure 4.11 except that the diameter of the hollow cathode hole is now 5 mm. The optimum amplitude of the X-ray pulse for this set of discharge is 8.6 V. It is obvious that the 5 mm diameter hollow cathode produces more intense electron beam. A comparison of the electron beam production in terms of electron beam target X-ray for the two setups with different hollow cathode diameter has been illustrated in Figure 4.11. As can be observed, the 5 mm diameter hollow cathode has higher amplitude X-ray pulse except at low operating pressure of 2.0×10^{-3} mbar. The optimum pressure is found to be at 1.5×10^{-2} mbar for both 1.5 mm and 5 mm diameter hollow cathode.

4.4 The Intensity of The Pre-Breakdown Electron Beam

Instead o f bombardment target, a charge collector was used as a detector for the electron beam. The result was taken at pressure of 1.5×10^{-2} mbar with charging voltage of –60 kV, as shown in Figure 4.12. As can be observed, the charge collector signal was obtained during the rising edge of dI/dt. This indicates that the

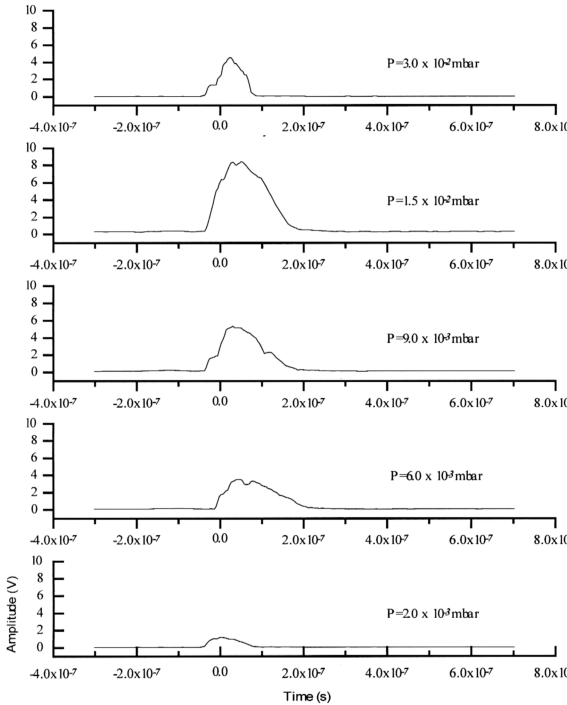

Figure 4.10 PIN diode output signals obtained at various pressures for 5 mm diameter hollow cathode.

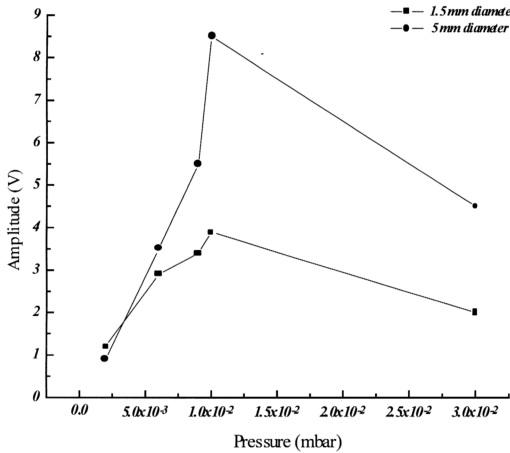

Figure 4.11 The comparison of the electron beam intensities for hollow cathode with diameter of 1.5 mm and 5 mm..

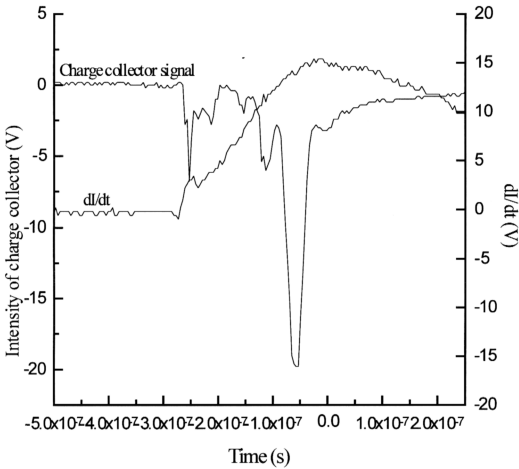

Figure 4.12 Charge collector and dI/dt signal obtained for discharge at –60 kV with pressures of 1.5×10^{-2} mbar.

emission of electron beam from the hollow cathode in pre-breakdown phase was recorded by the charge collector. This high energy electron beam corresponds to the electron beam that gives rise to the X-ray signal as can be seen in Figure 4.5 (b). But the charge collector also records some signals after the discharge has started and the X-ray signal has disappeared. This is because the charge collector is also sensitive to other sources such as UV light. The UV light source was emitted from the plasma. This plasma was created inside the discharge chamber during the discharge phase. Due to this complexity of mixed data, the charge collector is not suitable to be used to evaluate the emission of the electron beam during the breakdown phase.

The intensity of the electron beam during the pre-breakdown phase can be calculated from the signal of the charge collector during the rising edge of dI/dt. By integrating the first pulse of the charge collector signal, where the duration is 68 ns, a total electron charge of 3.0×10^{-7} C is obtained. This means that a total number of 1.9×10^{12} electrons are detected. The effective detection area of the charge collector is 3.3×10^{-5} m^2 (section 3.2). Hence, the minimum intensity of the electron beam is 9.1×10^{-3} Cm^{-2}. It is believed that the intensity of the electron beam is much higher than this value. This is because the diameter of the electron beam is expected to be much smaller than the effective area of the charge collector.

4.5 Measurement Of Electron Beam Energy

The electron beam energy is measured by X-ray foil absorption technique described in Chapter 3. Carbon disc is used as the bombardment target since the K_α of carbon has wavelength of 43.68 Å (corresponding to photon energy of 0.28 keV) so it can be rejected by using foil setups with cut off wavelength longer than 6 Å. Hence only the bremsstrahlung continuum will be detected.

Figure 4.13 shows the result obtained from a discharge at pressure 1.0×10^{-2} mbar, with the DXS system mounted on window W2 of the target chamber. The two foil combinations used in this setups are (i) 24 μm aluminised mylar and (ii) 24 μm aluminised mylar + 10 μm copper. The ratio of X-ray intensity transmitted through foil setup (i) to that of setup (ii) for carbon target is computed for electron beam energy from 16 keV to 68 keV by using equation 3.11 (Figure 4.14). The electron beam is assumed to be incident at 45^0 to the surface of the slanting carbon target, which has the thickness of 1 mm. The ratio decreases as the electron beam energy increases.

The temporal evolution of electron beam energy has been deduced for the system. The system is discharged at a voltage of -60 kV and at a pressure of 1.0 x 10^{-2} mbar. The diameter of the hollow cathode is 5 mm. Figure 4.15 shows the variation of the electron beam energy variation with time together with the two X-ray pulses from PIN diodes covered by the two foil setups. For this

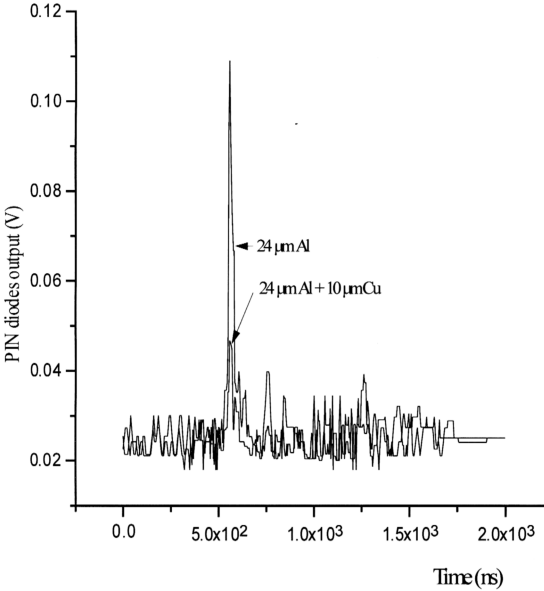

Figure 4.13 X-ray signals picked up by BPX-65 PIN diodes which are covered with 24 μm aluminised mylar and 24 μm aluminised mylar + 10 μm Cu at 1.0 x 10^{-2} mbar.

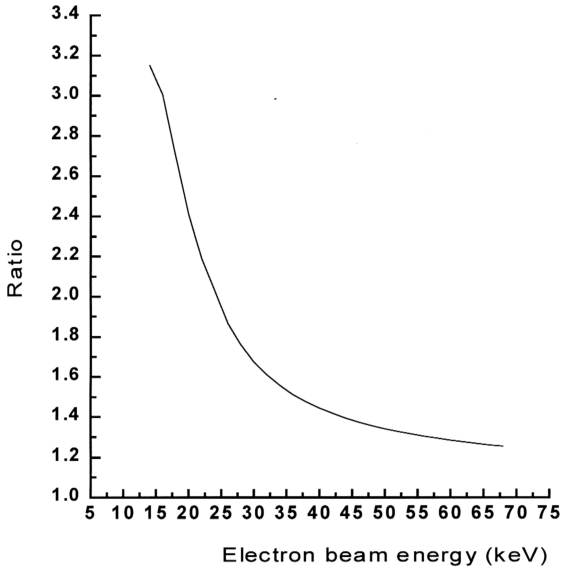

Figure 4.14 The graph of the ratio of X-ray intensity transmitted through 24 μm aluminised mylar to that of 24 μm aluminised mylar + 10 μm Cu as a function of electron beam energy for carbon target.

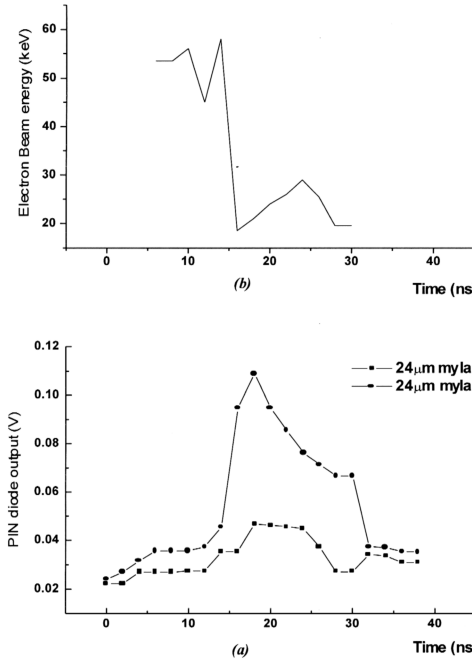

Figure 4.15 (a) The corresponding evolution of X-ray intensities detected simultaneously by two PIN diodes covered by (i) 24 μm aluminised mylar and (ii) 24 μm aluminised mylar + 10 μm Cu.

(b) The temporal variation of the electron beam energy in the pre-breakdown phase with discharge at -60 kV deduced from the X-ray signals in (a).

discharge, it can be observed that the electron beam energy maintains at around 50 keV before the sharp rising edge of the X-ray pulse. As the X-ray pulse is rising, the electron beam energy falls sharply to 18 keV and then increases again slowly. At the peak of the X-ray pulse, the beam energy is about 20 keV. Subsequently the electron beam energy and cannot be deduced accurately due to low X-ray intensities. However it is expected that the electron beam energy will decrease further since the sharp fall of the X-ray intensity also indicates the beginning of the main breakdown. During the breakdown, the plasma starts to develop inside the discharge chamber and the electric field at the inter-electrode space diminishes.

In Figure 4.16, another set of DXS signals from a discharge at pressure of 1.0 x 10^{-2} mbar are shown. The foil combination used to cover the BPX-65 diodes are (i) 12 μm aluminised mylar and (ii) 12 μm aluminised mylar + 10 μm copper. By using the same method as describe above, a graph of the time evolution of the electron beam energy is plotted in Figure 4.17. As can be observed, the temporal evolution of the electron beam energy is almost identical to that shown in Figure 4.15.

4.6 The Mechanism Of The Pre-breakdown Electron Beam Formation

The mechanism of the pre-breakdown electron beam formation can be

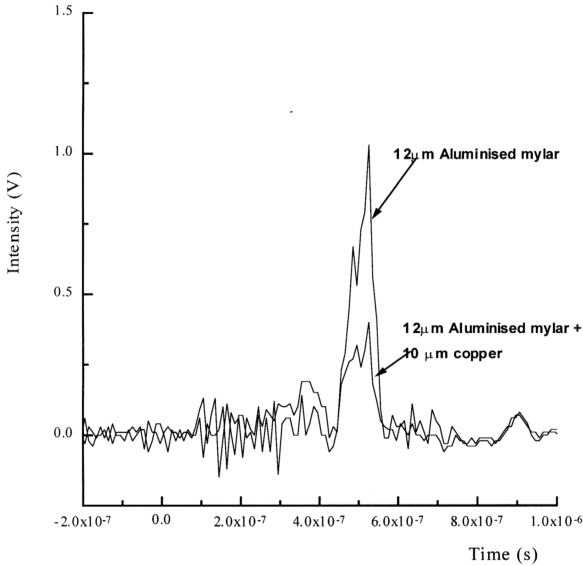

Figure 4.16 X-ray signals detected by BPX-65 PIN diodes covered by (i) 12 μm aluminised mylar and (ii) 12 μm aluminised mylar + 10 μm Cu at pressure of 1.5 x 10^{-2} mbar.

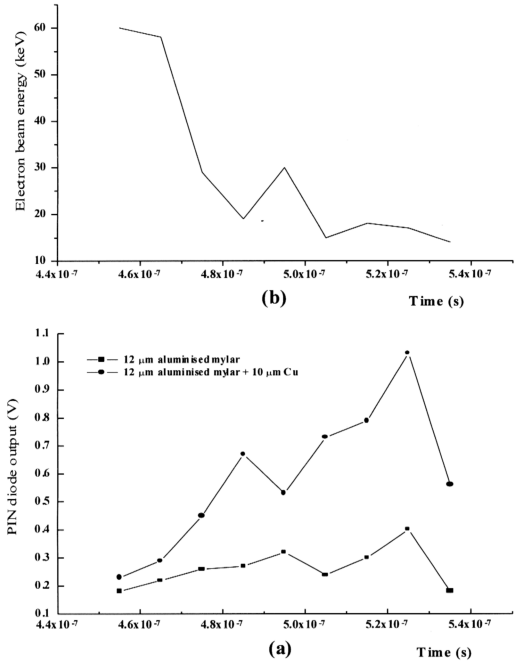

Figure 4.17 (c) The corresponding evolution of X-ray intensities detected simultaneously by two PIN diodes covered by (i) 12 μm aluminised mylar and (ii) 12 μm aluminised mylar + 10 μm Cu.

(d) The temporal variation of the electron beam energy in the prebreakdown phase with discharge at -60 kV deduced from the X-ray signals in (a).

explained based on Townsend discharge theory *[Townsend J. S., 1901]*. The pre-breakdown of the this system starts with some free electrons from the surface of the hollow cathode and accelerated towards the anode by the high voltage applied across the electrodes. Some of these electrons will collide and ionize the air molecules inside the hollow cathode region. This will generate more electrons which are accelerated towards the target. Fig. 4.4 shows that the intensity of the electric field is the highest along the axis of the hollow cathode. Most of the electrons will be collimated and move along the axis. The high energy electron beam from the hollow cathode will bombard and vapourize the anode. A plasma cloud is formed near the anode and it expands towards the hollow cathode. Due to the effect of polarization, charge separation will occur with this plasma cloud, and a virtual anode will be formed. When the plasma cloud expands close enough to the hollow cathode, an over-exponential growth in electron density will occur and then triggering a similar growth in the positive-ion density. This leads to the so-called avalanche.